An Analysis of Cloud Drop Growth by Collection: Part II. Single Initial Distributions[1]

EDWIN X BERRY

National Science Foundation, Washington, D. C. 20550

RICHARD L. REINHARDT

Sierra Nevada Corporation, Reno 89505

(Manuscript received 1 May 1974)

ABSTRACT

The initial spreading of a cloud droplet distribution, its time of formation and placement of the second maximum, and the value of the minimum between the two maxima are systematically related to the mean mass and standard deviation of the initial distribution.

1. Introduction

In Part I of this series (Berry and Reinhardt, 1974) we saw how the size distribution of droplets can be usefully divided into two separate spectra: Spectrum one (S1) which contains the smaller (cloud) droplets, and Spectrum two (S2) which contains the larger (large hydrometeor) drops. Later in this series (Parts 3 and 4) we will see that this division derives from the different values of the derivative of the collection kernel with respect to drop size in these two regions. In Part 1 we also described the model, the collection equation, and the new, highly accurate numerical method (Reinhardt, 1972) for the solution of this equation.

In this paper (Part II) we will take a closer look at how an initial S1 distribution of droplets evolves by collection into a bimodal (S1 plus S2) distribution. We will find that, for the range of initial conditions tested, there exist regularities in the spectrum evolution that can be expressed by simple algebraic equations. This is only an intermediate step, however, in our ultimate goal of being able to provide parameterized cloud physics equations for use in multi-array numerical cloud models. What we ultimately desire are not algebraic equations which depend upon the distribution properties at a pre-specified time, but rather rate equations that provide an estimate of the short-term evolution based upon the existing (at time t) properties of the distribution. Such rate equations will open the door to the superposition of the cloud processes, such as condensation, fallout, phase changes and mixing. As will be seen, we come closer to this goal in Parts III and IV of this series.

While it was first pointed out by Bartlett (1966) that initial spectra with fewer droplets produce large droplets faster, this paper shows a quantitative relationship between the rate of large drop production and the size and spread of the initial distribution for a selected general shape of initial distribution.

2. Primary parameters of the distribution[2,3]

Fundamental to discussions of droplet spectrum evolution are three extensive variables

$$N=\int f(x)dx, \tag{1}$$

$$L=\int xf(x)dx, \tag{2}$$

$$Z=\int x^2 f(x)dx, \tag{3}$$

three intensive variables

$$x_f=L/N, \tag{4}$$

$$x_g=Z/L, \tag{5}$$

$$x_b^2=x_f x_g-x_f^2, \tag{6}$$

and a relative variance

$$\text{var } x=x_b^2/x_f^2, \tag{7}$$

$$=(x_g/x_f)-1. \tag{8}$$

[1] See Part 1 for Acknowledgments.

[2] A more complete discussion is given in Part I.

[3] See Appendix for identification of symbols.

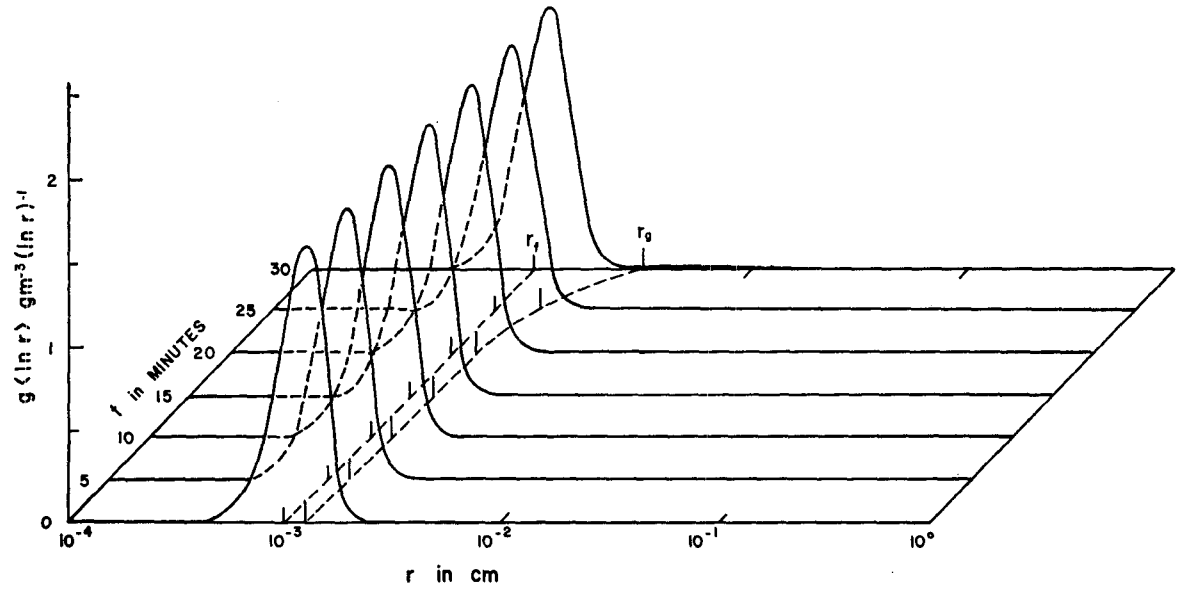

FIG. 1. Time evolution of the initial spectrum for $r_f^0 = 10\ \mu$m, var $x = 1$.

3. The initial distribution[4]

The initial density function used for these calculations is

$$f^0\langle x\rangle = N(x_f^0)^{-1}G(\nu)s^\nu e^{-(1+\nu)s}, \tag{9a}$$

$$s = x/x_f^0, \tag{9b}$$

$$G(\nu) = (1+\nu)^{1+\nu}/\Gamma(1+\nu), \tag{9c}$$

$$\text{var } x = (1+\nu)^{-1}. \tag{10}$$

The superscript zero indicates values at time zero.

The cases shown have $\nu = 0$, 3 which give a relative dispersion, var$^{\frac{1}{2}}x$, of 1, 0.5, respectively. The mean radius r_f takes the values of 10, 12, 14, 16 and 18 μm which, with the total liquid water content L of 10^{-6} gm cm^{-3}, corresponds to number densities N of 239, 166, 122, 93 and 74 cm^{-3}, respectively. Other values of

[4] This initial distribution [also used by Berry (1967) and Leighton and Rogers (1974)] is a generalization of Golovin's (1963) distribution as used by Scott (1968).

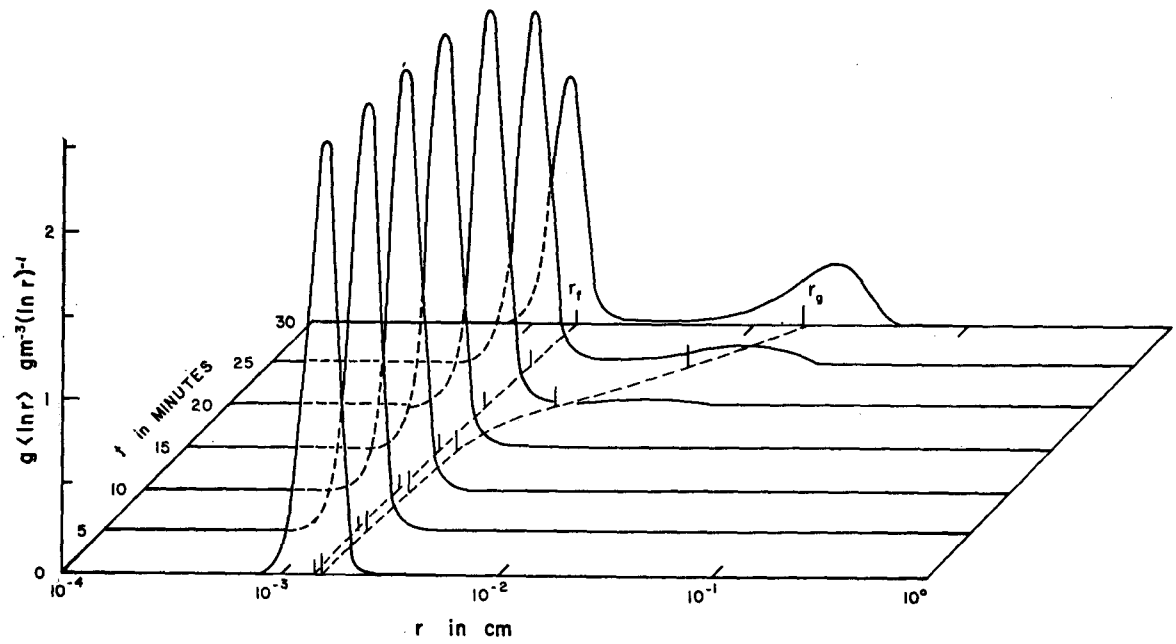

FIG. 2. Time evolution of the initial spectrum for $r_f^0 = 14\ \mu$m, var $x = 0.25$.

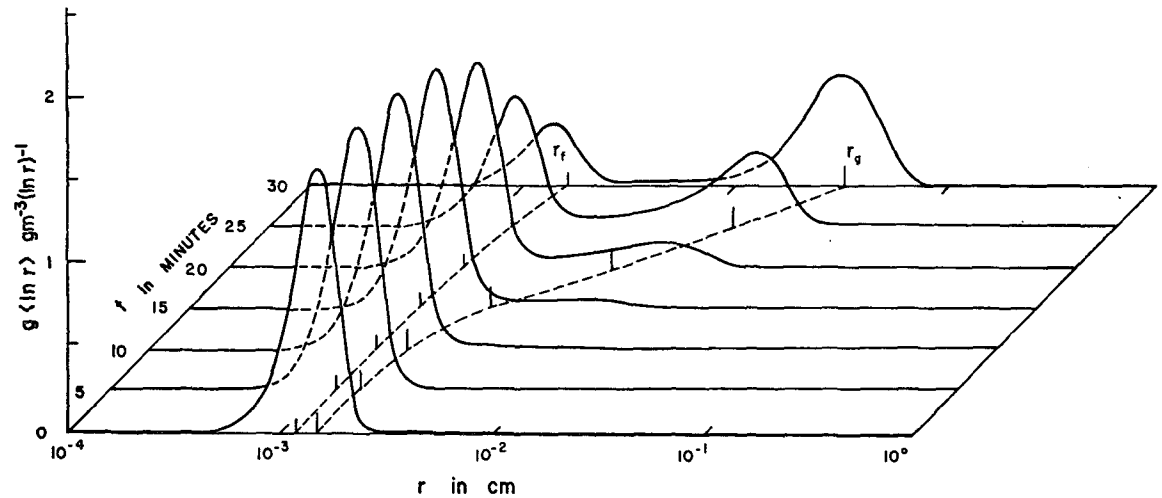

FIG. 3. Time evolution of the initial spectrum for $r_f^0 = 12\ \mu$m, var $x = 1$.

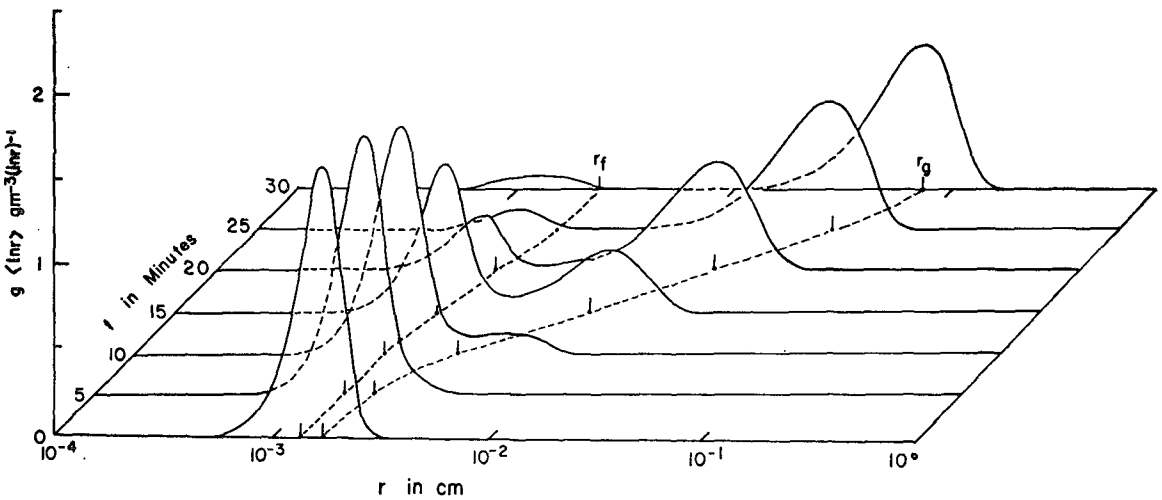

FIG. 4. Time evolution of the initial spectrum for $r_f^0 = 14\ \mu$m, var $x = 1$.

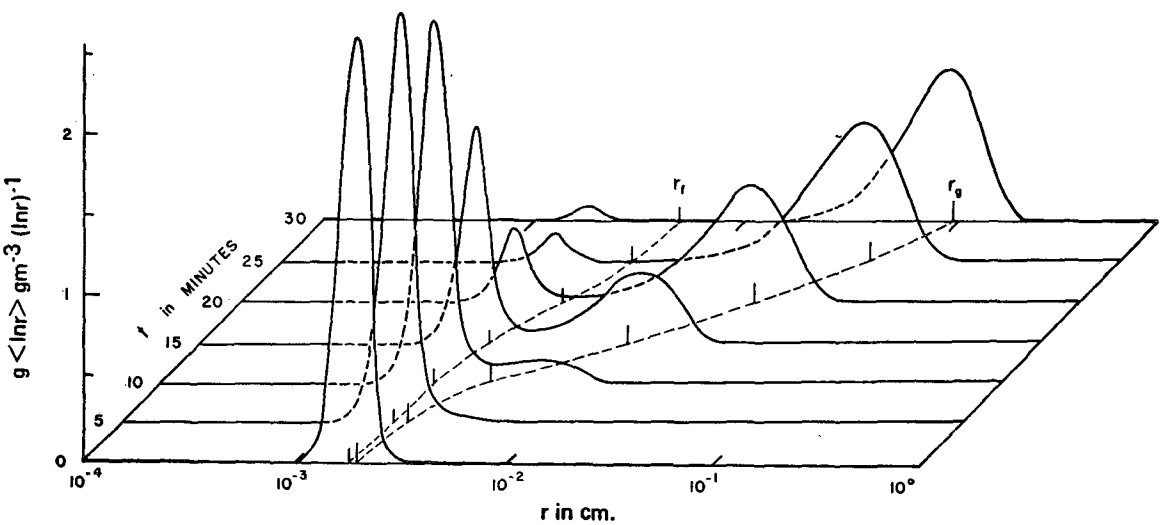

FIG. 5. Time evolution of the initial spectrum for $r_f^0 = 18\ \mu$m, var $x = 0.25$.

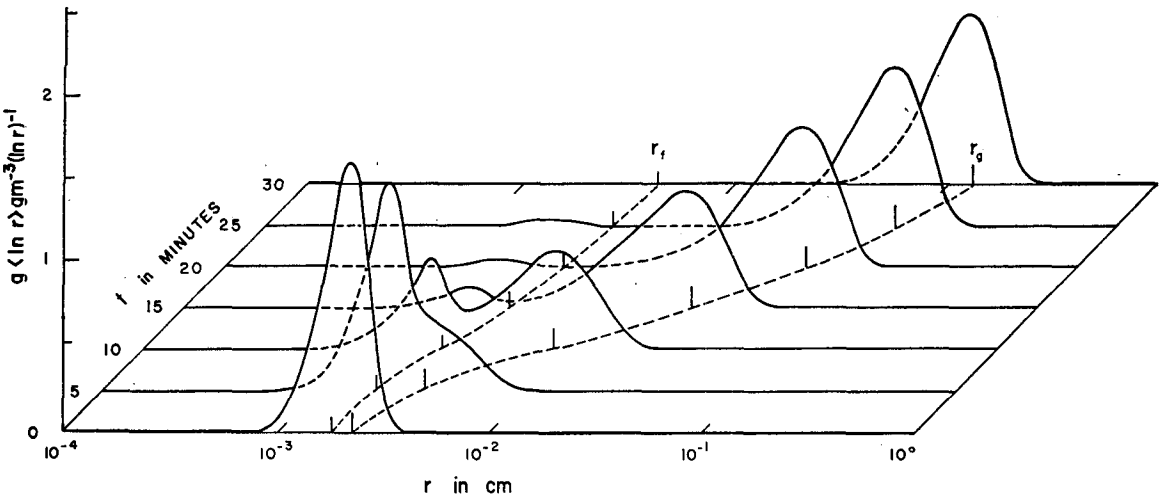

FIG. 6. Time evolution of the initial spectrum for $r_f^0 = 18$ μm, var $x = 1$.

TABLE 1. Data relating calculated parameters to initial values of Figs. 1–6.

r_f^0 (μm)	ν^0	r_0^0 (μm)	T (min)	T^{-1} (min^{-1})	T_2 (min)	T_2^{-1} (min^{-1})	g_m (10^{-6} gm cm^{-3})	L_2' (10^{-6} gm cm^{-3})	N_2' (cm^{-3})	T_H (min)	T_H^{-1} (min^{-1})	r_H (μm)	r_H^{-1} (10^2 cm^{-1})
10	0	10.0	32.0	0.031	25	0.040	0.35	0.019	0.039	28	0.036	100	1.00
14	3	11.1	22.5	0.044	18	0.056	1.07	0.044	0.076	20	0.050	80	1.26
12	0	12.0	19.2	0.052	14	0.072	3.0	0.047	0.23	16	0.062	71	1.42
16	3	12.7	15.8	0.063	12	0.084	3.9	0.077	0.32	14	0.071	71	1.42
14	0	14.0	13.0	0.077	9	0.11	10.0	0.090	0.29	11	0.091	63	1.59
18	3	14.3	12.0	0.083	9	0.11	9.7	0.130	0.36	10	0.10	63	1.59
16	0	16.0	9.6	0.104	7	0.14	23.1	0.175	0.83	8	0.12	50	2.00
18	0	18.0	7.7	0.130	6	0.17	39.0	0.269	0.90	7	0.14	45	2.25

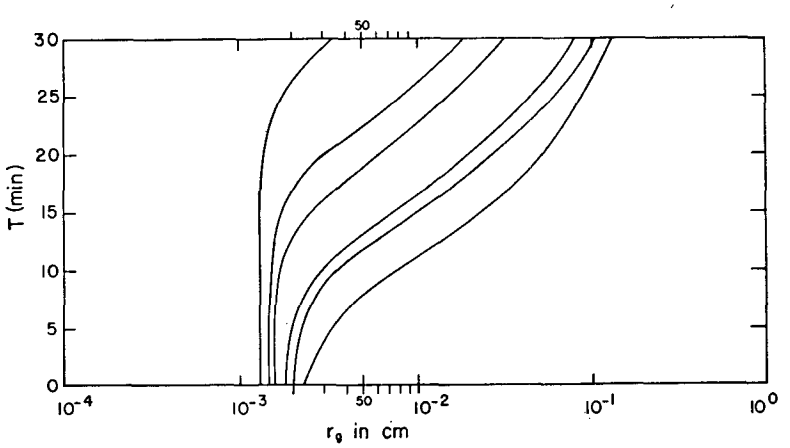

FIG. 7. Time change of r_g for the initial spectra of Figs. 1–6 shown in sequence from left to right:

1. $r_f^0 = 10$ μm, var $x = 1$.
2. $r_f^0 = 14$ μm, var $x = 0.25$.
3. $r_f^0 = 12$ μm, var $x = 1$.
4. $r_f^0 = 14$ μm, var $x = 1$.
5. $r_f^0 = 18$ μm, var $x = 0.25$.
6. $r_f^0 = 18$ μm, var $x = 1$.

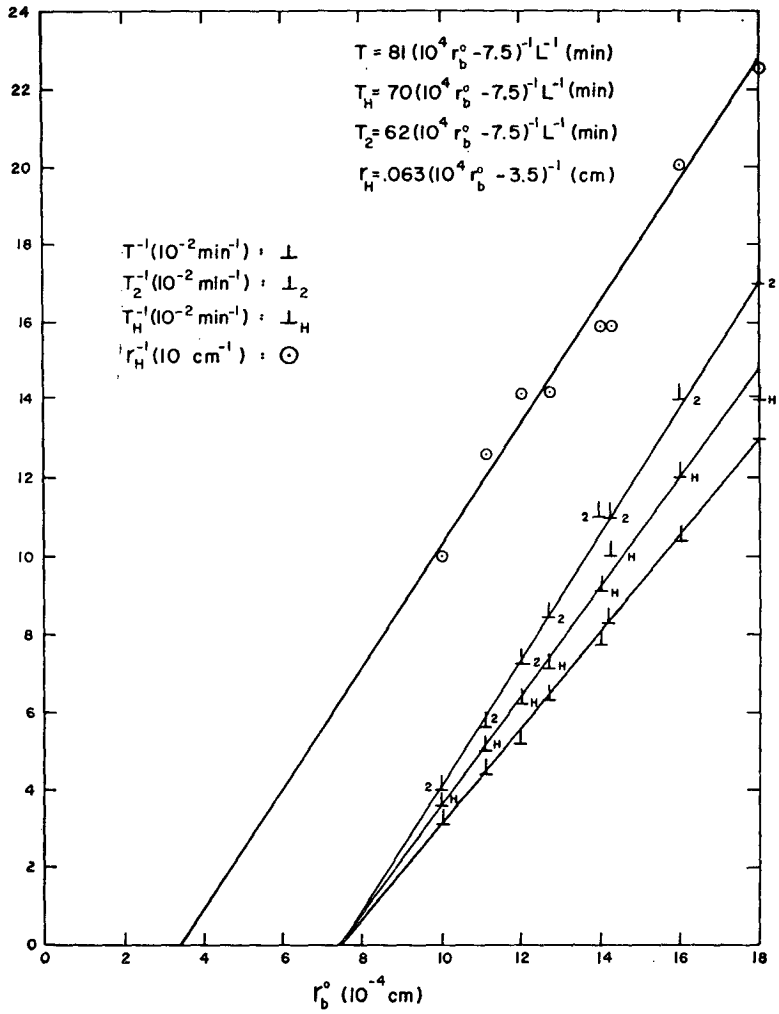

FIG. 8. The reciprocals of T, T_2 T_H, r_H plotted against r_b^0. Equations of the straight lines are given at the top of the figure; L is in gm m^{-3}.

L (and resulting proportional values of N) are accommodated in the parameterized equations to follow.

These calculations use the collision efficiencies of Hocking and Jonas (1970), which correspond to those of Davis and Sartor (1967), for $r \leqslant 40$ μm and those of Shafrir and Neiburger (1963) for $r > 40$ μm. All collisions are assumed to result in coalescence.

4. Growth of single distributions

Figs. 1–6 are six selected examples of the growth of a single initial distribution. The figures are ordered in terms of increasing r_b^0 as indicated in Table 1. These figures show that the production of large drops is significantly affected by both the initial mean radius and the initial relative dispersion.

Values of r_f and r_g are also plotted against time in Figs. 1–6. Since L is constant, the movement of r_f to the right is related to a decrease in N, and the movement of r_g to the right is associated with an increase in radar reflectivity. Note that as the spectrum evolves to its Golovin-like form (see Berry, 1967), r_g remains with the predominant water mass, while the commonly used mean radius r_f lags far behind.

All six r_g's are plotted together as a function of time in Fig. 7. Their growth patterns are similar but notice the dramatic dependence of the growth time on small differences in the initial r_g^0.

Only six cases are shown here. Some 30 others have been calculated and show the same pattern. (The r_g's have been found to cross in certain instances. Since x_f, as well as x_g, influences the growth rate, certain combinations of these two variables produce a crossing of the r_g's on a time plot.)

Let us define the following quantities:

T	time taken for r_g to reach 50 μm
T_2	time taken for r_{g2} to reach 50 μm
g_m	minimum value of $g\langle \ln r \rangle$ between S1 and S2 at time T_2

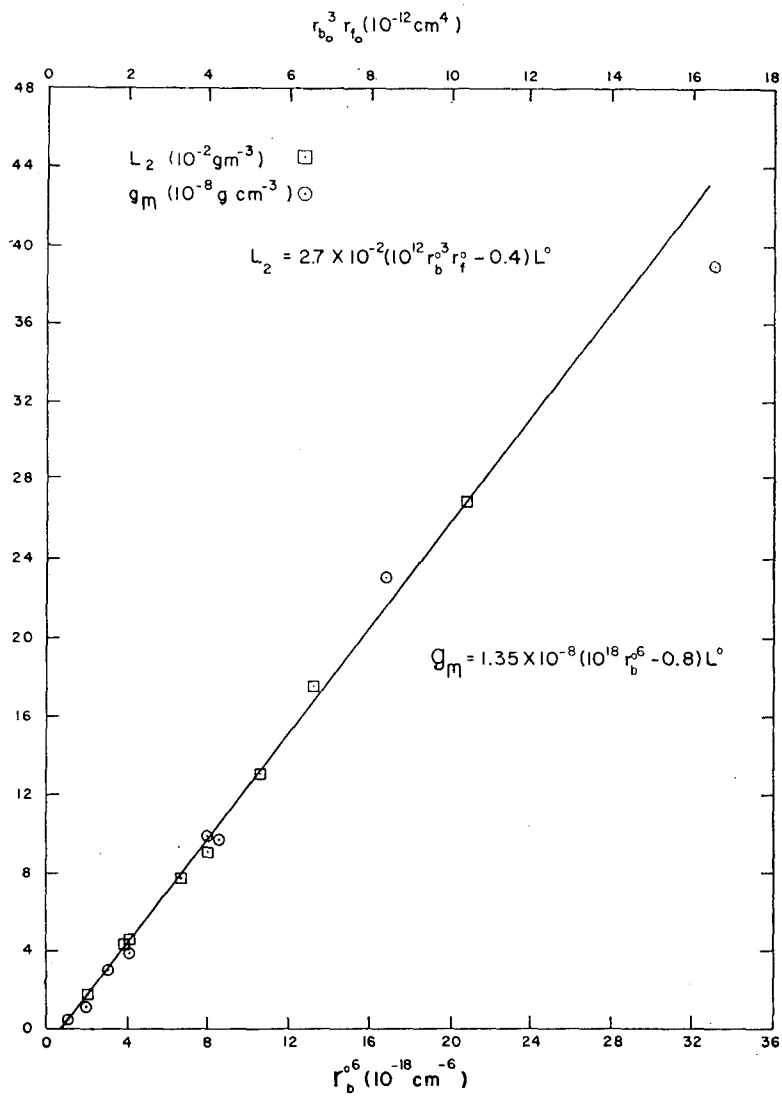

FIG. 9. The values of L_2 plotted against $(r_b{}^0)^3 r_f{}^0$ and g_m plotted against $(r_b{}^0)^6$. The same straight line applies in both cases. Equations for the straight line are given in the figure.

r_m	radius at which g_m occurs
r_{f2}'	value of r_{f2} at time T_2
$(\text{var}^{\frac{1}{2}}x)_2'$	value of $(\text{var}^{\frac{1}{2}}x)_2$ at time T_2
L_2'	value of L_2 at time T_2
N_2'	value of N_2 at time T_2
T_H	time at which the hump on S2 first forms
r_H	radius at which the hump on S2 first forms.

The values of these quantities have been calculated for Figs. 1–6.

In all cases, to a close approximation, we find:

$$r_m = 41\ \mu\text{m} \quad (11)$$

$$r_{f2}' = r_m \quad (12)$$

$$(\text{var}^{\frac{1}{2}}x)_2' = 1.0 \quad (13)$$

$$N_2' = 3.5\times10^6 L_2' \ [\text{gm}]. \quad (14)$$

These indicate that S2 at time T_2 has the same shape for all cases, although its size may differ as is seen from L_2 below. All other data are given in Table 1 and plotted in Figs. 8 and 9. The data may be approximated by the straight lines shown in the figures and given by the following equations:

$$T(\text{sec}) = 4.9\times10^{-4}(10^4 r_b{}^0 - 7.5)^{-1}L^{-1} \quad (15)$$

$$T_2(\text{sec}) = 3.7\times10^{-4}(10^4 r_b{}^0 - 7.5)^{-1}L^{-1} \quad (16)$$

$$g_m(\text{gm cm}^{-3}\text{ per ln}r) = 1.35\times10^{-8}[10^{18}(r_b{}^0)^6 - 0.8]L \quad (17)$$

$$L_2' = 2.7\times10^{-2}[10^{12}(r_b{}^0)^3 r_f{}^0 - 0.4]L \quad (18)$$

$$T_H(\text{sec}) = 4.2\times10^{-4}(10^4 r_b{}^0 - 7.5)^{-1}L^{-1} \quad (19)$$

$$r_H(\text{cm}) = 0.63(10^4 r_b{}^0 - 3.5)^{-1}. \quad (20)$$

It is interesting to note that the denominators of (15), (16) and (19) go to zero and T therefore to infinity when $r_b^0 = 7.5\ \mu$m. The data of Fig. 8, however, do not extend below $r_b^0 = 10\ \mu$m. The equations given are only one of several possible ways of fitting the data, but an effort has been made here for simplicity.

These parameterizations are based upon specific collection efficiencies and initial values in the range from $10\ \mu\text{m} \leqslant r_f^0 \leqslant 18\ \mu$m and $0.5 \leqslant (\text{var}^0)^{\frac{1}{2}} x \leqslant 1.0$. Until further calculations are completed, extrapolations of the equations given here beyond these limits should be made with care.

5. Comparison to double distributions

Since N, L and Z are extensive, the composite x_f and x_g of a double distribution may be found from (4) and (5) as follows:

$$x_f = \frac{L}{N_1+N_2} = \frac{1}{\dfrac{1}{x_{f1}}\left(\dfrac{L_1}{L}\right)+\dfrac{1}{x_{f2}}\left(\dfrac{L_2}{L}\right)}, \tag{21}$$

$$x_g = \frac{Z_1+Z_2}{L} = x_{g1}\left(\frac{L_1}{L}\right)+x_{g2}\left(\frac{L_2}{L}\right). \tag{22}$$

Since each component distribution of the double distributions of Part 1 had var $x = 1$, then using (8), $x_{g1} = 2x_{f1}$ and $x_{g2} = 2x_{f2}$. It follows from (6) that for Part 1 (Fig. 2) $r_b^0 = 20\ \mu$m, while $T = 2.0$ min; and for Part 1 (Fig. 3) $r_b^0 = 12.8\ \mu$m, while $T = 11.1$ min.

These points lie well above the T^{-1} line of Fig. 8. Therefore, the double distributions of Part 1, when taken as a sum-total single distribution, do not fit the pattern found here for single initial distributions. Their total relative dispersions, however [using (8)], are 1.73 and 6.25 for Part 1 (Figs. 2 and 3, respectively), which lie well outside the range tested here for single initial distributions.

6. Summary

The initial spreading of S1 due to self-collections has been shown to have a quantitative relationship to its mean mass x_{f1} and standard deviation x_b: if either is larger, the increase of x_{g2} is more rapid. The more rapid the increase of x_{g2}, the smaller will be the drops upon which the "second maximum" initially forms, and the greater will be the minimum value of $g\langle \ln r \rangle$ between the two maxima. This has been expressed quantitatively. This minimum value of $g\langle \ln r \rangle$ occurs at or near $r = 41\ \mu$m, and the variance of S2 as it is initially formed under the second maxima is unity.

APPENDIX

List of Symbols

f	number density function
g	mass density function
g_m	minimum value of $g\langle \ln r \rangle$ between S1 and S2 at time T_2
L	liquid water content
N	total number density
r	droplet radius
r_b	radius corresponding to $x_b = x_f(\text{var } x)^{\frac{1}{2}}$
r_f	radius corresponding to $x_f = L/N$
r_g	radius corresponding to $x_g = Z/L$
r_h	radius at which the hump on S2 first forms
r_m	radius at which g_m occurs
S1	the small hydrometeor or "cloud water" portion of the spectrum
S2	the large hydrometeor portion of the spectrum
T	time taken for r_g to reach $50\ \mu$m
T_H	time at which the hump on S2 first forms
var x	relative variance with respect to mass $[= (x_g/x_f)-1]$
x	droplet mass
x_b	standard deviation of mass about the mean x_f
x_f	mean mass of the number density function
x_g	mean mass of the mass density function
Z	spectral radar reflectivity, the second mass moment of the number density function
ν	width of spectrum parameter: var $x = 1/(\nu+1)$ for gamma number density function

REFERENCES

Bartlett, J. T., 1966: The growth of cloud droplets by coalescence. *Quart. J. Roy. Meteor. Soc.*, **92**, 93–104.

Berry, E. X, 1967: Cloud droplet growth by collection. *J. Atmos. Sci.*, **24**, 688–701.

——, and R. L. Reinhardt, 1974: An analysis of cloud drop growth by collection: Part I. Double distributions. *J. Atmos. Sci.*, **31**, 1814–1824.

Davis, M. H., and J. D. Sartor, 1967: Theoretical collision efficiencies for small cloud droplets in Stokes flow. *Nature*, **215**, 1371–1372.

Golovin, A. M., 1963: The solution of the coagulating equation for cloud droplets in a rising air current. *Bull. Acad. Sci. USSR, Ser. Geophys.*, No. 5, 482–487.

Hocking, L. M., and P. R. Jonas, 1970: The collision efficiency of small drops. *Quart. J. Roy. Meteor. Soc.*, **96**, 722–729.

Leighton, H. G., and R. R. Rogers, 1974: Droplet growth by condensation and coalescence in a strong updraft. *J. Atmos. Sci.*, **31**, 271–279.

Reinhardt, R. L., 1972: An analysis of improved numerical solutions to the stochastic collection equation for cloud droplets. Ph.D. dissertation, University of Nevada.

Scott, W. T., 1968: Analytic studies of cloud droplet coalescence 1. *J. Atmos. Sci.*, **25**, 54–65.

Shafrir, U., and M. Neiburger, 1963: Collision efficiencies of two spheres falling in a viscous medium. *J. Geophys. Res.*, **68**, 4141–4147.